

Article

# The Influence of Cation Treatments on the Pervaporation Dehydration of NaA Zeolite Membranes Prepared on Hollow Fibers

Xuechao Gao <sup>\*,†</sup>, Bing Gao <sup>†</sup>, Xingchen Wang, Rui Shi, Rashid Ur Rehman  and Xuehong Gu <sup>\*</sup>

State Key Laboratory of Materials-Oriented Chemical Engineering, College of Chemical Engineering, Nanjing Tech University, 5 Xinmofan Road, Nanjing 210009, China; gb123456789@njtech.edu.cn (B.G.); xingchenwang@njtech.edu.cn (X.W.); 15062281631@njtech.edu.cn (R.S.); dr.rehman@njtech.edu.cn (R.U.R.)

<sup>\*</sup> Correspondence: xuechao.gao@njtech.edu.cn (X.G.); xhgu@njtech.edu.cn (X.G.); Tel.: +86-25-8317-2268 (X.Gu)

<sup>†</sup> The authors contribute equally to this work.

Received: 21 April 2018; Accepted: 23 May 2018; Published: 1 June 2018



**Abstract:** NaA zeolite membrane is an ideal hydrophilic candidate for organic dehydrations; however, its instability in salt solutions limits its application in industries as the membrane intactness was greatly affected due to the replacement of cation ions. In order to explore the relationship between the structural variation and the cation types, the obtained NaA zeolite membranes were treated by various monovalent and divalent cations like  $\text{Ag}^+$ ,  $\text{K}^+$ ,  $\text{Li}^+$ ,  $\text{NH}_4^+$ ,  $\text{Zn}^{2+}$ ,  $\text{Mg}^{2+}$ ,  $\text{Ba}^{2+}$  and  $\text{Ca}^{2+}$ . The obtained membranes were subsequently characterized by contact angle, scanning electron microscopy (SEM), pervaporation (PV), and vapor permeation (VP). The results showed that all of the hydrophilicities of the exchanged membrane were reduced, and the membrane performance varied with cation charges and sizes. For the monovalent cations, the membrane performance was largely determined by the cation sizes, where the membrane remained intact. On the contrary, for the divalent cation treatments, the membrane separation was generally reduced due to the presence of cation vacancies, resulting in some unbalanced stresses between the dispersive interaction and electrostatic forces, thereby damaging the membrane intactness. In the end, a set of gas permeation experiments were conducted for the two selected cation-treated membranes ( $\text{K}^+$  and  $\text{Ag}^+$ ) using  $\text{H}_2$ ,  $\text{CO}_2$ ,  $\text{N}_2$  and  $\text{CH}_4$ , and a much higher decreasing percentage (90% for  $\text{K}^+$ ) occurred in comparison with the permeation drop (10%) in the PV dehydration, suggesting that the vaporization resistance of phase changing for the PV process was more influential than the water vapor transport in the pore channel.

**Keywords:** NaA zeolite membrane; pervaporation; cation treatments; membrane separation; hollow fibers

## 1. Introduction

Fuel ethanol is considered as a promising alternative to the conventionally used fossils due to its significant advantages in terms of environment protection, energy intensity, and resource abundance [1–3]. At present, microbial fermentations are the mainstream route that is used in the industry to produce fuel ethanol; however, by-products and water generated during the fermenting activities [4] should be removed simultaneously in order to maintain the production efficiency. Among the diverse separation strategies, the membrane-based pervaporation (PV) process, as a newly emerging technique, has attracted considerable attention due to its significant advantages of less energy consumption and operational convenience over the traditional separation methods, such as extraction and distillation.

In general, the membranes that are used for organic dehydrations can be classified into two categories, which include (i) polymeric and (ii) inorganic membranes. Although the polymer is easy to fabricate due to its high flexibility, it suffers from weak mechanical strengths and swelling problems,

thereby limiting its application [5–7]. Not only has the inorganic membrane demonstrated good mechanical strengths, but also strong chemical resistance and high thermostability were also derived, so it is more promising to be used in harsh solutions containing additives, like dimethylformamide (DMF), tetrahydrofuran (THF) and salts. Among the various types of inorganic membranes, zeolite membrane, making use of its unique pore structure and surface properties, are widely deployed for organic dehydrations [8]. In the past two decades, many types of zeolites have been fabricated as the supported zeolite membranes [7,9], including LTA [10,11], FAU [12], T [13], MOR [14] and MFI [15–17]. Among these candidates, The tubular NaA zeolite membrane has been widely applied in pharmaceutical and food industries for solvent recoveries [18]. NaA zeolite contains sodium cations, and the chemical formula is  $\text{Na}_{12}[(\text{AlO}_2)_{12}(\text{SiO}_2)_{12}] \cdot 27\text{H}_2\text{O}$  [19], where the sodalite cages are connected through double four-membered rings (4MR) in order to form a large cavity. For the NaA zeolite membrane with a Si/Al ratio of 1.0, high permselectivities can be achieved due to its strong hydrophilicity. Since the first commercial application of tubular NaA membranes in practical factories by Mitsui Engineering and Shipping in the 1990s, over 200 sets of the membrane plants have been established in the world for various purposes [20–22]. However, the tubular NaA membrane often contains large diameters and thick walls, so the packing density and flux in a certain membrane module are limited, thereby increasing the membrane facility investment.

To further reduce the membrane cost, the packing density of the membrane module should be significantly increased. Therefore, there is an on-going effort to prepare the NaA membrane on hollow fibers with a much smaller diameter and thinner walls. However, at present, the NaA membranes prepared on the hollow fiber are still unsatisfactory due to their low selectivity. This could be caused by the high curvature of the substrate surface, which induces stresses between the membrane and substrate surface, thereby leading to the presence of the inter-crystalline defects [23,24]. Therefore, it is necessary to use chemical approaches to improve the membrane performance in order to increase the adhesive forces between the membrane layer and substrate. To fix the membrane defects derived during the preparation, cations exchanges could be employed to cover interstitial gaps by changing the crystal cell parameters, which resulted in the contraction and expansion of the zeolite particles. Further, inorganic salts are generally presented in organic solvents used in the fields of organic chemicals, fine chemicals, and pharmaceutical chemicals. The salts inevitably interacted with the NaA zeolite and thus affected the separation performance of the NaA zeolite membrane by changing the zeolite structure and surface hydrophilicity. According to the work by Breck and co-workers [25], the pore size of LTA zeolite could be tailored using various cation treatments. For the zeolite that was treated by potassium, the effective pore size was reduced to 0.28 nm; on the contrary, the calcium salt produced a larger pore size of 0.51 nm. Francisco et al. [26] investigated several ion-exchanged NaA/carbon membranes for hydrogen purification, and it had found that the Rb-LTA and Cs-LTA/carbon membranes provided better separation performance. Shirazian et al. [27]. Prepared the K-exchanged LTA zeolite membranes for the dehydration of natural gas; however, the separation factors were still close to the prediction of Knudsen diffusion. Yang et al. studied the influence of several inorganic salts on the PV performance for the ethanol/H<sub>2</sub>O/salt mixtures, and a significant flux drop was found, which was assumed to be caused by the pore blocking and surface precipitation of salts [28–31]. However, the above research only involved a limit number of cations, and the membrane structural changes caused by the cation exchanges were not explicitly correlated with the ionic size and charge, but were lumped with the driving force variations and transport resistance increments during the PV characterization.

Based on above discussion, it is necessary to scientifically and systematically explore the relationship of separation variations with cation sizes and charges using both PV dehydration and gas permeation techniques, so as to provide guidance in order to broaden the industrial application of hollow fibered supported NaA zeolite membranes. In this paper, we prepared hollow fiber supported NaA zeolite membranes in a batch mode with acceptable separation performances, which was later treated by different cations solutions (monovalent and divalent cations) to derive ion-exchanged NaA zeolite membranes. Then, the ion-exchanged membranes were characterized by PV for 90 wt %

ethanol/water solution. The variations of permeation fluxes and selectivities were studied and were used to correlate the coordinated effect between the cation size and charge. In the end, the PV decrement for several cation treatments was compared with that for the gas permeation and vapor permeation (VP) tests to evaluate the importance of the surface hydrophilicity and the vaporization resistance of the NaA zeolite membranes for water molecules.

## 2. Experimental

### 2.1. Materials

The monovalent and divalent salts (monovalent: NaCl, LiCl, NH<sub>4</sub>Cl, KCl and AgNO<sub>3</sub>; divalent: ZnCl<sub>2</sub>, MgCl<sub>2</sub>·6H<sub>2</sub>O, CaCl<sub>2</sub> and BaCl<sub>2</sub>) were purchased from commercial companies, and they were used as received without any purification. The silica sol, water glass and NaAlO<sub>2</sub> were used as Si and Al sources with industrial purity. The original NaA zeolite seeds (cubic crystals, with a size of 2–4 μm) and deionized water were produced in the laboratory. The alumina four channel hollow fibers (4CHF) were used as the support (homemade, out diameter: 3.4–3.8 mm, length: 70 mm, porosity: 45–55%).

### 2.2. Synthesis of NaA Zeolite Membranes and Ion-Exchange Processes

The preparation process of NaA crystal suspension: 0.2 g silica sol was added to a certain amount of ball-milled NaA zeolite crystal solution so as to improve the viscosity and to prevent the agglomeration of seeds; after that, the solution was mixed by an ultrasonic cell grinder (power 200 W) for 30 min, in order to obtain a uniformly dispersed seed suspension. Seeding the hollow fiber: the hollow fibers, soaked with 0.1 mol·L<sup>-1</sup> sodium hydroxide solution for 12 h, were placed in a 60 °C oven and were dried overnight; after that, the hollow fibers were pre-coated by the dip-coating method for 5–15 s.

The preparation process of the NaA zeolite membrane was provided in Figure 1. At the beginning, the sodium hydroxide that was dissolved in deionized water to provide basic conditions, was later mixed with sodium aluminate to derive a clear solution, and then a certain amount of water glass was added into the mixture under vigorously stirring for 1.5 h, where the molar ratio of the synthesis solution is Al<sub>2</sub>O<sub>3</sub>:SiO<sub>2</sub>:NaOH:H<sub>2</sub>O = 1:2:2:120. Subsequently, the treated supports that were vertically placed in a Teflon-stainless steel autoclave containing the synthesis sol, were transferred into the oven for 4 h at 100 °C. The as-synthesis membrane was washed with deionized water several times, before drying at 70 °C overnight.

The preparation of ion-exchanged NaA-type zeolite membrane: the 90% ethanol/water solution was mixed with a certain amount of NaCl, LiCl, NH<sub>4</sub>Cl, KCl, AgNO<sub>3</sub>, ZnCl<sub>2</sub>, MgCl<sub>2</sub>, CaCl<sub>2</sub>, or BaCl<sub>2</sub>, respectively, to derive a mixture with a salt concentration of 0.05 mol/L–0.10 mol/L by sonicating for 30 min; the ion-exchange solution was pumped into the liner that was equipped with the prepared NaA zeolite membrane to exchange for 24 h at 50 °C. After the exchanging, the membrane was immersed in deionized water for 2 h, and was then was dried for characterizations.

The preparation of ion-exchanged NaA zeolite powder: the salt solutions were prepared according to the above method, and then 40 g of the salt solution and 0.6 g NaA crystal were stirringly mixed in a conical flask immersed in a water bath of 50 °C for 4 h. After the exchanging, the suspension was centrifuged for several times and dried.

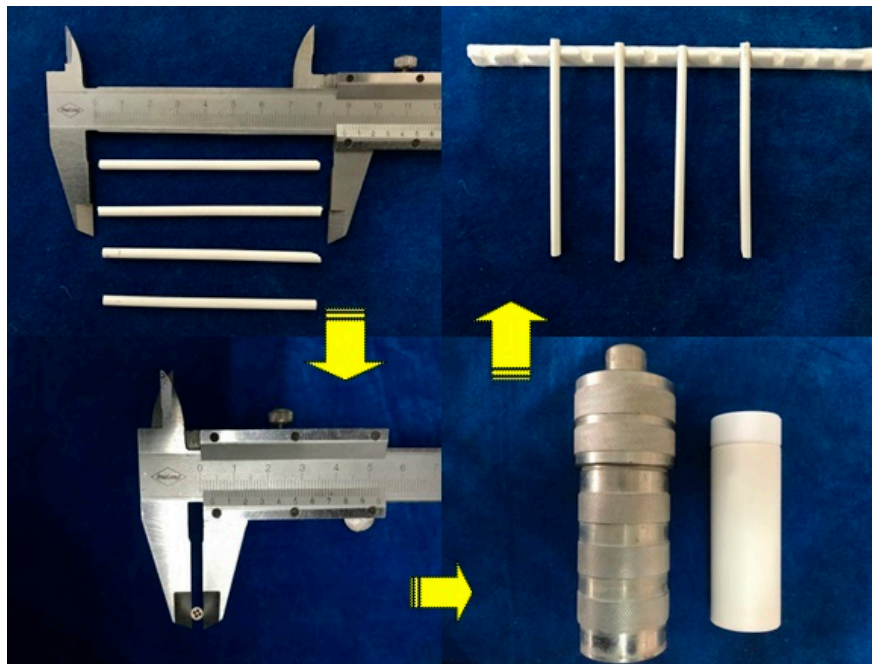


**Figure 1.** Cation treatment diagram of NaA zeolite membranes.

### 2.3. Characterization of NaA Zeolite Particles and Membranes

The morphologies of the as-synthesis NaA zeolite powders and membranes were characterized by field emission scanning electron microscopy (FESEM) and installed with a cold field emission gun that was operating at 5 kV and 10  $\mu$ A (S-4800, Hitachi, Tokyo, Japan). The crystal structure of the sample was analyzed by X-ray diffraction (XRD) at a tube voltage of 40 kV and a tube current of 15 mA (MiniFlex 600, Rigaku, Tokyo, Japan), where the Cu target and the Ni filter were used to generate  $K\alpha$  rays and to remove  $K\beta$  rays, respectively. The tests were performed at room temperature with a diffraction range of  $5^\circ$ – $50^\circ$ , and a scan rate of  $12^\circ$ /min. After exchanging, the elemental content of the sample was measured by inductively coupled plasma optical emission spectrometry (ICP-OES, optima 7000DV, PerkinElmer, Waltham, MA, US), where the samples were dissolved in an acidic mixture before testing.

### 2.4. PV Test and Single Gas Permeation

The separation performances of NaA zeolite membranes were evaluated by dehydrating 90 wt % ethanol-water solution at  $75^\circ\text{C}$  by a PV apparatus, as reported in our previous work [32]. The compositions of the feed and permeate were analyzed by gas chromatography (GC-6890, Ruihong, Tengzhou, China). The PV performance of each membrane was determined by the separation factor ( $\alpha$ ) and flux ( $J$ ), which were, respectively, defined as follows:

$$\alpha = \frac{y_w/y_e}{x_w/x_e} \quad (1)$$

$$J = \frac{m}{A \cdot \Delta t} \quad (2)$$

where  $y_w$  and  $y_e$  are the mass fractions of water and ethanol in the permeate, respectively;  $x_w$  and  $x_e$  correspond to the fraction values in the feed, respectively;  $m$  is the mass (kg) permeated over a time period of  $\Delta t$  (h); and,  $A$  is the effective membrane area ( $\text{m}^2$ ).

By excluding the influence of the membrane hydrophilicities, gas permeation at room temperature was used to characterize the importance of the vaporization effect in the NaA zeolite membranes

that were treated by different cations. For the permeation experiment, the membrane was sealed by silicone O-rings and the volumetric flow rates of single gases ( $H_2$ ,  $CO_2$ ,  $CH_4$  and  $N_2$ ) were measured using a bubble flow meter. The tested gas on the feed side provided a driving force for gas permeation from the outside of the membrane to the lumen inside, where the gas permeation flux ( $Pm_i$ ) can be expressed as:

$$Pm_i = \frac{n}{A \cdot \Delta t \cdot \Delta P} \quad (3)$$

where  $Pm_i$  represents the molar quantity of the gas flowing through the membrane per unit time and per unit area under per unit pressure difference ( $\text{mol} \cdot \text{m}^{-2} \cdot \text{h}^{-1} \cdot \text{Pa}^{-1}$ );  $n$  corresponds to the moles of the gas; and,  $\Delta P$  is the pressure difference (Pa).

### 3. Results and Discussion

#### 3.1. PV Performances of the Exchanged NaA Zeolite Membrane

Figure 2 depicted the ion exchange model for the NaA zeolite with high aluminum content to show how different cation affects the open pore passages. As suggested, cation charges affect the exchange number of ions during the exchange in order to maintain the valence balance of the zeolite. According to the law of conservation of charge, each divalent cation consumes two replacements of monovalent sodium ion, and vice versa. In the cation treatment, in order to ensure the full exchange of ions with the membrane, an exchanging time of 24 h and a cation concentration of 0.1 mol/L were firstly selected. To initially examine the effect of ion exchanges of different cations on the membrane performance, both the feed and permeate were analyzed by a gas chromatograph, where the PV solution was a 90 wt % ethanol/water mixture.

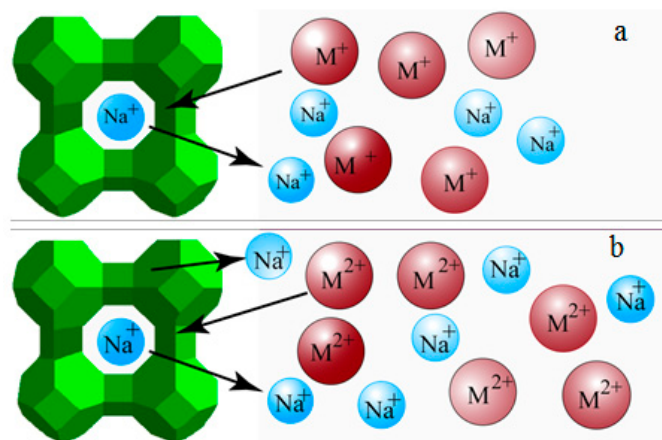


**Figure 2.** Different cation exchange model of the NaA-Type zeolite. (a) Monovalent cation and (b) Divalent cation.

Table 1 summarized the PV results for different salts, where the corresponding cation sizes were provided in Table 2. As suggested, the kinetic radii of the monovalent cations, like  $K^+$  and  $Ag^+$  (1.49 Å and 1.26 Å), are greater than that of  $Na^+$  (1.17 Å), and the PV separation factor of the membrane was increased and the permeate flux was decreased. This is probably because  $K^+$  or  $Ag^+$  entered into zeolite cage and replaced the original  $Na^+$ , which resulted in the decrease in accessible pore size. Smaller pores yielded lower permeation fluxes, but higher separation factor. For the smallest monovalent cation ( $Li^+$ ), when the original  $Na^+$  was replaced by  $Li^+$ , the pore was significantly opened, which led to a much higher permeate flux, but without any selectivity during the PV test. For the treatment by the acidic cation solution of  $NH_4Cl$ , both the permeation flux and the separation factor were considerably reduced, suggesting that the membrane structure was significantly changed. The decrease in the permeation flux could be explained by the ionic size effect (1.48 Å versus 1.17 Å), where the water

passage in the membrane was blocked by the larger cation. The decrease in the separation factor was caused by the chemical attack to the zeolite skeleton due to the presence of H proton that was released from the cation for the  $\text{NH}_4\text{Cl}$  solution being acidic. On the other hand, the surface precipitation of salts on the membrane surface could also cause the decrease of permeation flux. To evaluate such an effect, the NaCl solution was used as a reference. As given in the Table 1, before and after the treatment with NaCl solution, the permeation flux and the separation factor of the membrane only change slightly, so the surface precipitation effect could be neglected in the experiment.

For the divalent cations of  $\text{Mg}^{2+}$  and  $\text{Zn}^{2+}$  with smaller ion sizes (0.72 Å and 0.74 Å), both the permeation flux and the separation factor of the NaA zeolite membranes dramatically decreased after cation exchanging. This was because of the displacement of  $\text{Na}^+$  cations around the six-membered ring-like structures. When the  $\text{Na}^+$  ions were deprived from zeolite pores by the smaller divalent cations of  $\text{Mg}^{2+}$  and  $\text{Zn}^{2+}$ , the open pore size became larger than the molecular size of ethanol, so the separation factor was reduced. In addition, since the molar ratio of ion exchanging between  $\text{Na}^+$  and  $\text{Mg}^{2+}/\text{Zn}^{2+}$  was 2, the remaining cation sites in the zeolite were vacancies, so some unbalanced stresses were induced, where the membrane porosity was reduced due to some collapse. When the effect of porosity decrement outweighed the effect that was caused by the pore enlargement, the overall permeation flux still decreased. For the other two divalent cations ( $\text{Ca}^{2+}$  and  $\text{Ba}^{2+}$ ) with larger ion sizes (1.0 Å and 1.35 Å), the coordinated effect between open pore size and unbalanced stresses due to cation vacancies were similar except the pore size that was caused by  $\text{Ba}^{2+}$  treatment became smaller. The decrease in open pore size should cause the increase in the separation factor; however, the unbalanced stresses generated some defects between crystals in the membrane, so the membrane intactness was reduced, which caused the decrease in the separation factor. Another evidence for the presence of defects in the  $\text{Ba}^{2+}$  treatment was the increase in flux.

**Table 1.** Pervaporation of 90 wt % ethanol/water mixture through NaA-type zeolite membrane and its cation-exchanged membrane (exchange condition: 12 h at 60 °C and cation concentration of 0.1 M).

Ion Valence State	Material	Processing Conditions	Fluxes/kg·m <sup>-2</sup> ·h <sup>-1</sup>	Separation Factor
1	KCl	Un-exchange	4.05 ± 0.019	449 ± 2.4
		Exchange	3.58 ± 0.023	1062 ± 12.8
	$\text{NH}_4\text{Cl}$	Un-exchange	7.42 ± 0.023	306 ± 1.1
		Exchange	1.44 ± 0.005	38 ± 0.1
	LiCl	Un-exchange	4.58 ± 0.019	208 ± 0.5
		Exchange	leaking	1 ± 0.01
	NaCl	Un-exchange	4.75 ± 0.023	449 ± 2.4
		Exchange	4.83 ± 0.018	519 ± 3.1
	$\text{AgNO}_3$	Un-exchange	6.51 ± 0.027	548 ± 3.6
		Exchange	5.98 ± 0.025	2136 ± 50.7
2	$\text{MgCl}_2$	Un-exchange	5.05 ± 0.025	2167 ± 52.5
		Exchange	1.99 ± 0.014	47 ± 0.1
	$\text{BaCl}_2$	Un-exchange	4.80 ± 0.024	208 ± 0.6
		Exchange	5.19 ± 0.025	162 ± 0.4
	$\text{CaCl}_2$	Un-exchange	6.45 ± 0.025	306 ± 1.2
		Exchange	6.07 ± 0.024	52 ± 0.1
	$\text{ZnCl}_2$	Un-exchange	5.06 ± 0.019	2156 ± 53.4
		Exchange	2.90 ± 0.015	5 ± 0.04

**Table 2.** The cation radius of the used salts.

Cations	Hydrated Radius, Å [33]	Bare Radius, Å [34]
Li <sup>+</sup>	3.82	0.94
Na <sup>+</sup>	3.58	1.17
K <sup>+</sup>	3.31	1.49
Ag <sup>+</sup>	3.41	1.26
NH <sub>4</sub> <sup>+</sup>	3.31	1.48
Mg <sup>2+</sup>	4.28	0.72
Ca <sup>2+</sup>	4.12	1.00
Ba <sup>2+</sup>	4.04	1.35
Zn <sup>2+</sup>	4.30	0.74

### 3.2. Surface Morphology of the Exchanged NaA Zeolite Membrane

To further testify the above structural alternations, which gave rise to the changes in permeation fluxes and separation factors, the surface morphologies of NaA zeolite membranes after various cation treatments were examined by the scanning electron microscopy (SEM) technique. The obtained images for the monovalent cation treatment were depicted in Figure 3. As suggested, no large cracks of crystal particles and interstitial defects were found on the surface of the zeolite membrane after being treated with 0.1 M AgNO<sub>3</sub>, NaCl, KCl and NH<sub>4</sub>Cl solutions, so the membranes intactness was maintained in the cation treatments. When compared to the feature of the original NaA zeolite crystals in Figure 3a, no significant changes occurred to the samples that were treated with KCl and NaCl solutions in Figure 3b,f. Further, for AgNO<sub>3</sub> treatment in Figure 3c, a large amount of amorphous substances were found on the membrane surface, which may be caused by the partial destruction of particle due to the crystal cell expansion by the replacement of Ag<sup>+</sup>, i.e., the interstitial defects between the particles were largely fixed, which increased the separation factor but decreased the permeation flux. However, for the NH<sub>4</sub>Cl treatment in Figure 3d, the zeolite crystals on the membrane surface started to dissolve as the sharp edges of the crystal particles were absent. This was largely due to the dealumination in the zeolite framework under acidic conditions (NH<sub>4</sub>Cl solution is acidic), thereby resulting in collapses of the skeleton and the partial dissolution of the membrane. For the smallest monovalent cation treatment of LiCl in Figure 3e, no amorphous substances were found on the membrane surface, and the crystal shapes remained unchanged except with larger interstitial spaces due the crystal cell contraction, which may be responsible for the membrane leaking in the PV tests in Table 1.

The SEM images for divalent cation treatments were provided in Figure 4, where the crystal shapes were unaffected, with larger interstitial spaces. However, for the treatment by BaCl<sub>2</sub> solution in Figure 4b, some amorphous substances were found on the membrane surface. Similar to the explanation for AgNO<sub>3</sub>, the amorphous substances were generated by the cell expansion due to the replacement of larger ionic sizes of Ba<sup>2+</sup>. Since the interstitial gaps were covered, the separation factor was slightly increased. As the PV results given in Table 1, the coordinated effect between the pore blocking effect and the minimization of intercrystals gaps by the amorphous substance led to the slight variation of PV performances of NaA zeolite membrane treated by Ba<sup>2+</sup>. However, for other small divalent cations, due to the unbalanced exchange number between Na<sup>+</sup> and M<sup>2+</sup>, some cation sites in the zeolite structure were left vacant, so some porosities of crystals were lost due to the structural collapse, which resulted in a complex behavior of fluxes and separation factors.

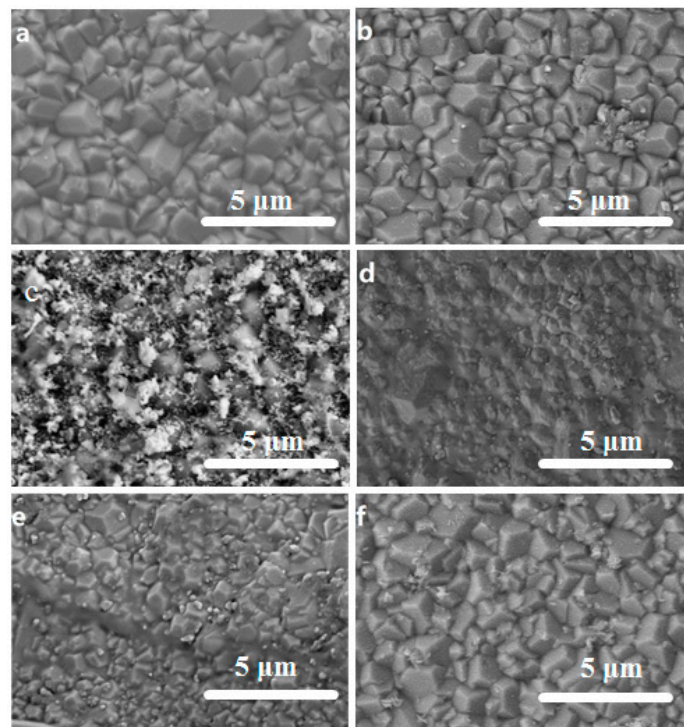


**Figure 3.** Scanning electron microscopy (SEM) images of NaA zeolite membrane (a) and its cation treated surface morphologies by (b) KCl, (c) AgNO<sub>3</sub>, (d) NH<sub>4</sub>Cl, (e) LiCl and (f) NaCl solutions.

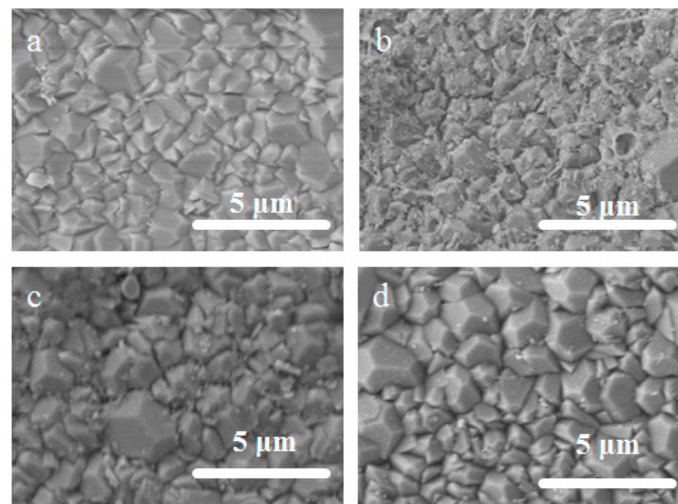


**Figure 4.** SEM images of NaA zeolite membrane surface morphologies treated by (a) CaCl<sub>2</sub>, (b) BaCl<sub>2</sub>, (c) ZnCl<sub>2</sub> and (d) MgCl<sub>2</sub> solutions.

### 3.3. The Structural Analysis of the Exchanged NaA Zeolite Powders

Due to the replacements of new cations, not only were the cell parameters of NaA zeolite crystals changed to some extent, but also new substances were obtained, which in turn led to the variation of permeation flux and separation factors, and such a variation could be confirmed by the XRD characterization. Figure 5 illustrated the XRD results for the cation treated zeolite particles. As suggested in Figure 5a, the XRD peak intensities of the sample that was treated by AgNO<sub>3</sub> were dramatically reduced, suggesting the presence of amorphous substances. In Figure 5b, a similar trend also occurred in the sample that was treated by Ba<sup>2+</sup>, so the interpretation for the membrane surface

morphologies was validated. In general, the PV performances of divalent cation treated NaA zeolite membrane were unsatisfactory. For  $Mg^{2+}$ ,  $Ca^{2+}$  and  $Zn^{2+}$  ion treatments, both the permeation flux and the separation factor of the membrane decreased, which had little change in  $Ba^{2+}$  treatment. For the monovalent cation treatments, the permeation fluxes of the membrane after the exchange of  $Ag^+$  and  $K^+$  slightly decreased, but the separation factor has been greatly improved. Therefore, the variation trends of the membrane performance after  $M^{2+}$  exchange depended on the coordinated effect between porosity losses and ionic sizes, where a smaller ionic size generally reduced the membrane porosity due to structural collapse, and such an effect could be inhibited in the case for larger size cations due to a stronger dispersive interaction. For monovalent cations, in addition to the acidic/basic condition, the ionic size played a dominating role in the predication of membrane performance variations as no cation site was left vacant after exchanging treatments.

By observing the variations of crystal morphologies and the cation contents for the powder sample, a deeper understanding of ion exchanging could be achieved for the membranes. Table 3 illustrated that the ICP characterization results for the treated and original NaA zeolite crystals. It could be found that the content of  $Na^+$  only increased slightly after NaCl solution treatment. However, according to the conservation of charge, the content of  $Na^+$  should be unchanged in theory. The possible reasons were due to the presence of a small amount of residual ions in the crystals. For other cations, the content of  $Na^+$  steadily decreased. For the monovalent salts, about 90%, 16% and 59% of  $Na^+$  was replaced by  $Ag^+$ ,  $Li^+$  and  $K^+$ , respectively. In comparison, for the divalent salts, about 78%, 49%, 66% and 81% of  $Na^+$  were replaced by  $Zn^{2+}$ ,  $Mg^{2+}$ ,  $Ca^{2+}$  and  $Ba^{2+}$ , respectively. In addition, the relative molar content of the positive charge was very close to 1 for all of the samples, matching well with the NaA zeolite structure.

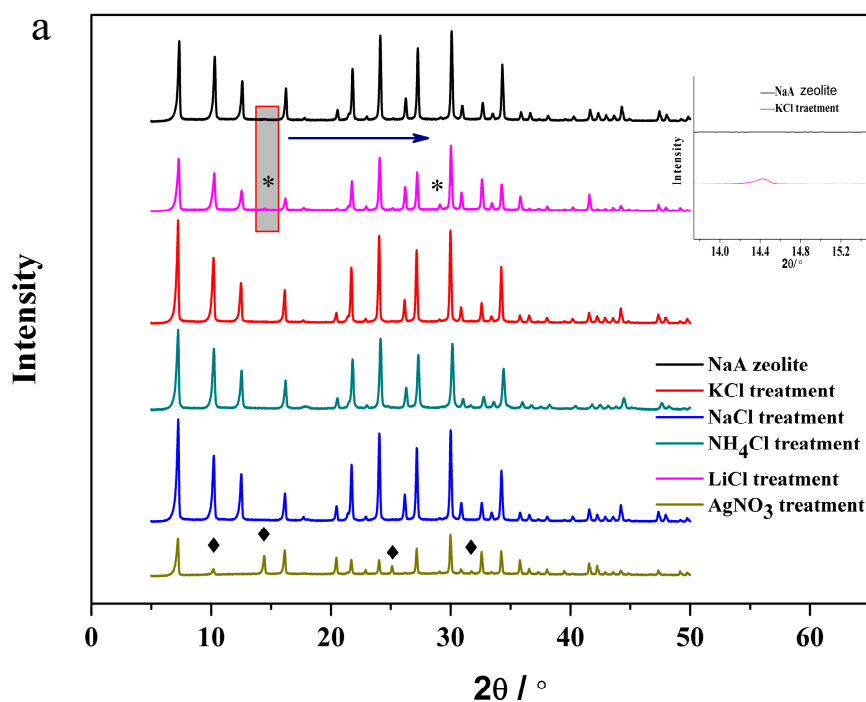
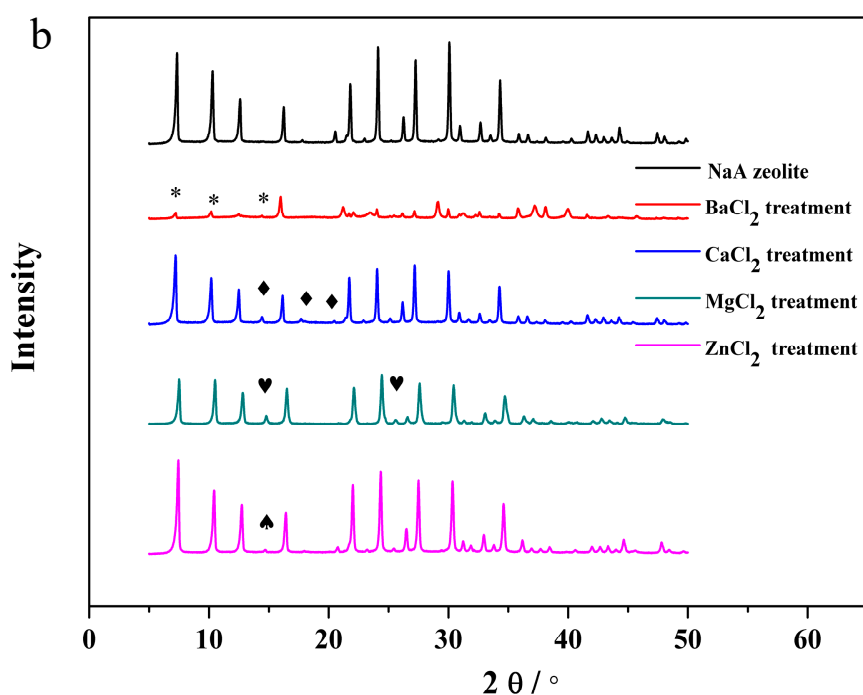


Figure 5. Cont.



**Figure 5.** X-ray diffraction (XRD) patterns of NaA zeolite seeds and after treatment seeds with (a) monovalent cations and (b) divalent cations.

**Table 3.** Inductively coupled plasma (ICP) tests of NaA zeolites treated by different cations.

Type	Relative Content of Na	Relative Content of Positive Charge <sup>a</sup>
NaA zeolite	1.00	0.96
NaCl treatment	1.12	1.03
LiCl treatment	0.84	0.93
KCl treatment	0.41	0.97
AgNO <sub>3</sub> treatment	0.10	0.99
ZnCl <sub>2</sub> treatment	0.22	0.97
MgCl <sub>2</sub> treatment	0.51	1.06
CaCl <sub>2</sub> treatment	0.34	1.02
BaCl <sub>2</sub> treatment	0.19	0.99

<sup>a</sup> [(Na<sup>+</sup> + M<sup>+</sup>)/Al or (Na<sup>+</sup> + 2M<sup>2+</sup>)/Al]. Each element represents its molar content.

Since the cations were successfully incorporated in the NaA zeolites, the SEM technique was used to examine the morphology changes of the crystals, with the results being summarized in Figure 6. As suggested in Figure 6b,e,f, the salts of KCl, NaCl and LiCl had no destructive effects on the crystals; on the contrary, the crystals after the AgNO<sub>3</sub> treatment were rounded in some way (Figure 6c), as the distinct edges became blurred due to swelling. For the NH<sub>4</sub>Cl treatment in Figure 6d, the crystals became less distinctive and smaller, indicating that acidic fluid dissolved the crystalline structures. Based on above discoveries, it was evident that the influence of Ag<sup>+</sup> on the NaA zeolite structure was relatively significant, which was consistent with the discoveries that were based on the SEM image for AgNO<sub>3</sub> solution in Figure 4b. Further, after the divalent salt treatments by CaCl<sub>2</sub>, BaCl<sub>2</sub>, ZnCl<sub>2</sub> and MgCl<sub>2</sub> solution in Figure 6g–j, not only did some damages occur to the particles during the replacements of cations, but also a small amount of amorphous substances were found on the crystal surface, which may be related to the flux decrement in the treated membranes, i.e., pore blocking effect due to the porosity loss.

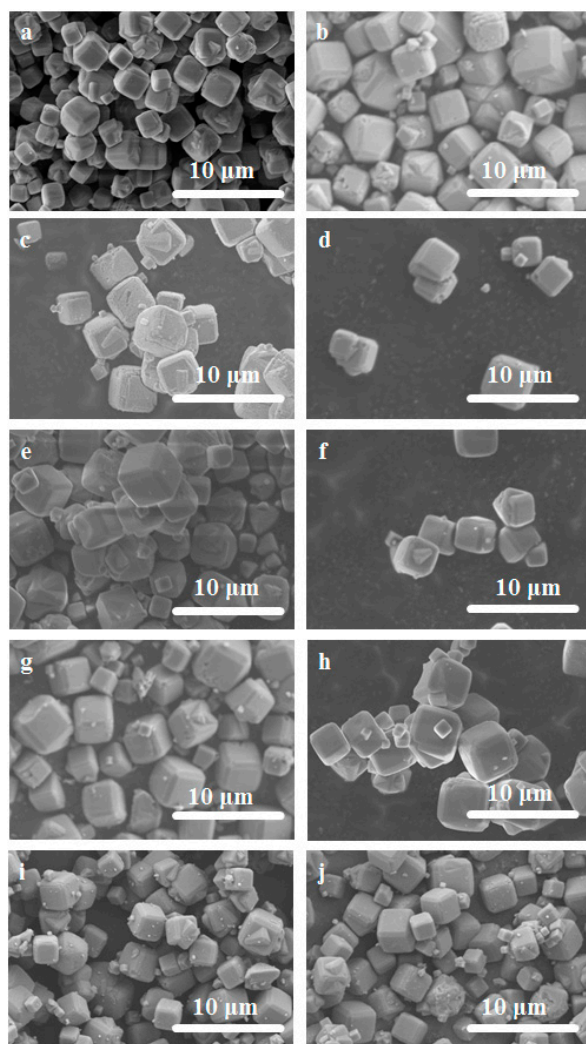


**Figure 6.** SEM images of NaA zeolite particles (a) and ion-exchanged zeolite with (b) KCl, (c) AgNO<sub>3</sub>, (d) NH<sub>4</sub>Cl, (e) LiCl, (f) NaCl, (g) CaCl<sub>2</sub>, (h) BaCl<sub>2</sub>, (i) ZnCl<sub>2</sub> and (j) MgCl<sub>2</sub> solution treatment.

#### 3.4. The Concentration Effect on the Exchanged Membrane

Since the PV performance of the NaA zeolite membrane that was treated by divalent cations was not improved, only the concentration effect of monovalent cations on the PV performance was explored for the exchanged membrane. Table 4 summarized that the PV performances of different NaA zeolite membranes that were treated by various monovalent cations with several concentrations. For a high concentration of 0.10 M, it was evident that the separation factor of the NaA zeolite membrane was greatly improved after conducting KCl, AgNO<sub>3</sub> exchanging, where the decrease in the flux was caused due to the pore blocking effect of K<sup>+</sup> and Ag<sup>+</sup> cations. For the lower concentrations of K<sup>+</sup> and Ag<sup>+</sup> with a value of 0.05 M, the membrane separation factors were still very high (>10,000), and the corresponding fluxes became 4.45 and 5.87 kg·m<sup>-2</sup>·h<sup>-1</sup>, respectively, which were slightly lower than that for the original NaA zeolite membrane (4.96 kg·m<sup>-2</sup>·h<sup>-1</sup> and 6.51 kg·m<sup>-2</sup>·h<sup>-1</sup>, respectively). This was due to the faster exchanging rate with Na<sup>+</sup> ions that was caused by the higher concentration. As the highest separation factor occurred to the mild concentration, it was reasonable to conclude that higher exchanging rate may also induce some unbalanced structural variations in the membrane. Similarly, the exchange effect of NH<sub>4</sub>Cl at a concentration of 0.05 M is better than that of 0.1 M by PV characterization. This was caused by the stronger acidity of the 0.1 M NH<sub>4</sub>Cl solution, which dissolved the membrane layer to some extent. For LiCl, no differences were obtained for the two conditions

as the leakages occurred due to the smaller kinetic diameter of  $\text{Li}^+$ , which permitted both water and ethanol molecules passing through the membranes. Based on the PV results for the treated NaA-type zeolite membranes, it was evident that the concentration of 0.05 M was more suitable for  $\text{Ag}^+$  and  $\text{K}^+$  to fix the membrane defects.

**Table 4.** Pervaporation (PV) performances of the NaA zeolite membranes treated by various concentrations of monovalent cation solutions, by dehydrating 90 wt % ethanol/water mixture.

No.	Cations	Concentration/M	Flux/kg·m <sup>-2</sup> ·h <sup>-1</sup>	Separation Factor
M1	-	-	4.96 ± 0.03	449 ± 2.4
M1'	K <sup>+</sup>	0.05	4.45 ± 0.02	>10,000 ± 198.2
M1''	K <sup>+</sup>	0.1	3.58 ± 0.02	1062 ± 12.8
M2	-	-	6.51 ± 0.03	548 ± 3.6
M2'	Ag <sup>+</sup>	0.05	5.87 ± 0.03	>10,000 ± 198.2
M2''	Ag <sup>+</sup>	0.1	5.98 ± 0.03	2136 ± 50.9
M3	-	-	7.42 ± 0.03	306 ± 1.2
M3'	NH <sub>4</sub> <sup>+</sup>	0.05	4.95 ± 0.02	107 ± 0.2
M3''	NH <sub>4</sub> <sup>+</sup>	0.1	1.44 ± 0.01	38 ± 0.1

The SEM images of the NaA membranes that were treated by different concentrations were shown in Figure 7. It was observed that the ion exchanging rate difference due to the cation concentration clearly occurred to  $\text{Ag}^+$  and  $\text{NH}_4^+$  in Figure 7a,b and Figure 7c,d due to the larger cation sizes, which yielded a limited exchanging rate. For the size identical cation of  $\text{K}^+$  in Figure 7e,f, and the difference between the two conditions was negligible due to the close similarity of crystals in two conditions.

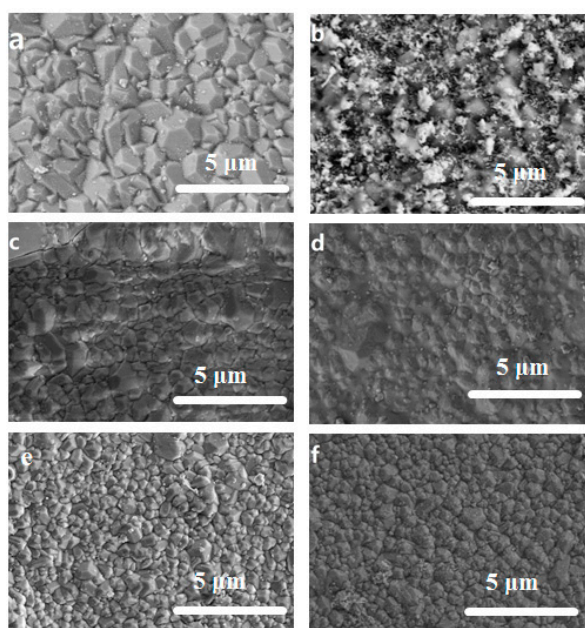


**Figure 7.** SEM images of NaA zeolite membrane treated by different concentration cations of  $\text{AgNO}_3$  (a) 0.05 M, (b) 0.1 M,  $\text{NH}_4\text{Cl}$  (c) 0.05 M, (d) 0.1 M,  $\text{KCl}$  (e) 0.05 M and (f) 0.1 M.

### 3.5. PV Stability Test of NaA Zeolite Membrane

Since improved performances were found for the monovalent salts of  $\text{KCl}$  and  $\text{AgNO}_3$ , respectively, the PV stability tests were conducted for the treated NaA zeolite membranes that were derived under a salt concentration of 0.05 M for 24 h at 60 °C. The results were shown in Figure 8. As given in Figure 8a for  $\text{KCl}$ , the flux increased after the first immersing. This was due to the initial dissolution of some amorphous substance on the membrane surface, where the membrane intactness

and the crystal structure were affected. Since a lower transport resistance occurred, the flux was increased without affecting the separation factor. After the secondary immersing, the membrane flux increased from  $4.96 \text{ kg}\cdot\text{m}^{-2}\cdot\text{h}^{-1}$  to  $7.6 \text{ kg}\cdot\text{m}^{-2}\cdot\text{h}^{-1}$ . This could be explained that the amorphous substances dissolved in the solution exposed the interstitial defects, thereby increasing the flux but reducing the selectivity. After the third immersing, the PV performance tended to be stable, where the flux remained at  $6.5 \text{ kg}\cdot\text{m}^{-2}\cdot\text{h}^{-1}$ , with the water content as high as 99.7%. In total, within 220 h, the KCl-exchanged NaA membrane maintained adequate fluxes with enough water purity in the permeate (above 99.6 wt %), and no significant damages occurred to the membrane. For the durability test of  $\text{Ag}^+$  exchanged zeolite membrane in Figure 8b, the flux tended to decrease significantly with the extension of operation time. This was caused by the preferential adsorption of water molecules on the membrane surface, leading to the blockage of the pore channel, thereby, resulting in a decrease in flux. However, after immersing in the raw material fluid for a long time, the flux increased due to a partial dissolution and destruction of the amorphous material on the membrane surface. Since the membrane intactness was still neat, the permeate purity was hardly affected. In total, the NaA zeolite membrane that was treated with  $\text{Ag}^+$ , could keep a high performance in the PV test in 230 h. Since the amorphous substances were crucial to the performance evolution for the ion-exchanged membranes, the Energy-dispersive X-ray spectrometry (EDX) analysis was used to detect its chemical compositions, and the corresponding results were provided in Figure 9. As suggested, besides the elements (K or Ag) from the salts, the elements of Al, Si and O were also found, so the amorphous substances on the membrane surface were regarded as aluminosilicate.

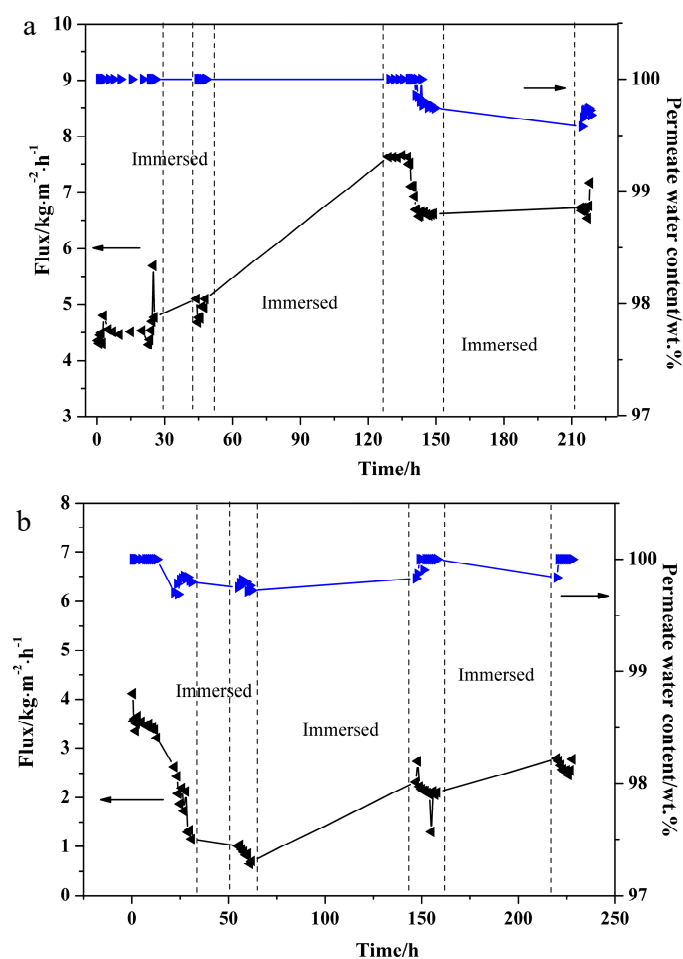


**Figure 8.** PV dehydration of 90 wt % ethanol/water mixture with different cation-treated NaA zeolite membranes (a) KCl solution treatment, (b)  $\text{AgNO}_3$  solution treatment.

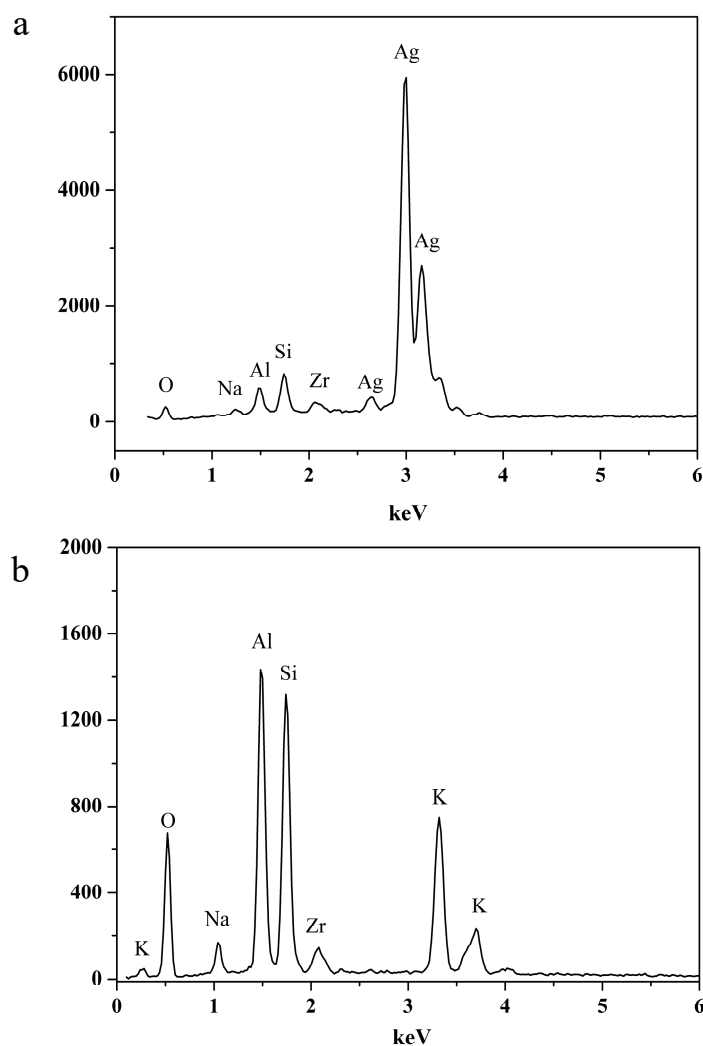


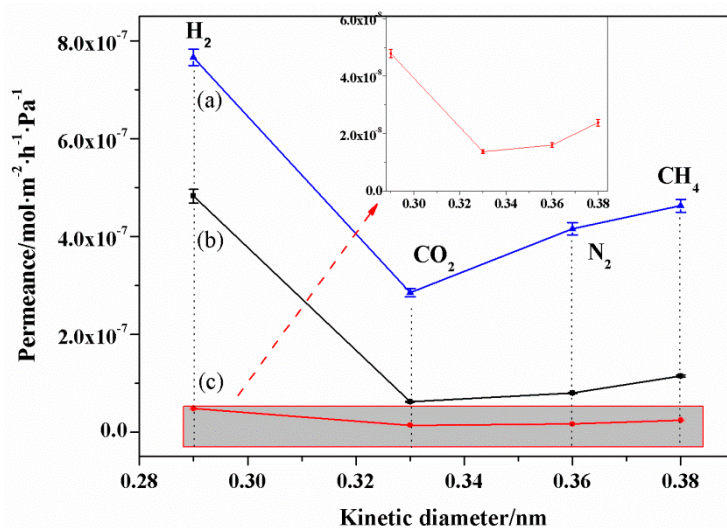
**Figure 9.** Energy-dispersive X-ray spectrometry (EDX) analysis for different cation-treated NaA zeolite membranes (a)  $\text{AgNO}_3$  solution treatment, (b) KCl solution treatment.

### 3.6. Gas Permeation of NaA Zeolite Membranes

NaA zeolite membranes have exhibited high performance in liquid separation, but it has to admit that the membrane performance for gas separation is still far below the expectation, as the non-zeolitic pores and defects permit gas molecules passing through the membrane layer via Knudsen diffusion rather than by molecular sieving [22]. However, the gas permeation characterization provides effective insights for the structural changes in the membrane layer by excluding the hydrophilicity variation of the membrane surface due to the cation exchanges. In order to further elucidate the relative importance of the pore channel variation on NaA zeolite membrane due to the cation replacement, the contact angle was first used to inspect the variation of membrane hydrophilicity, and such a result was provided in Table 5. As suggested, all the hydrophilicities of the exchanged NaA zeolite membranes were considerably reduced in comparison with that of the original membrane, suggesting interplay between the pore variation and hydrophilicities in the complex behaviour of the exchanged membrane that was treated by different cations.

The gas permeation test was carried out on NaA ion-exchanged membrane with good PV dehydration performances, and the blocking effect of  $\text{Ag}^+$  and  $\text{K}^+$  was determined by the changes of permeance. Figure 10 illustrated the variation of permeance through the membrane as a function of the kinetic diameter of gases, using a driving pressure of 2.0 bar at 25 °C, where flow rates of single gases

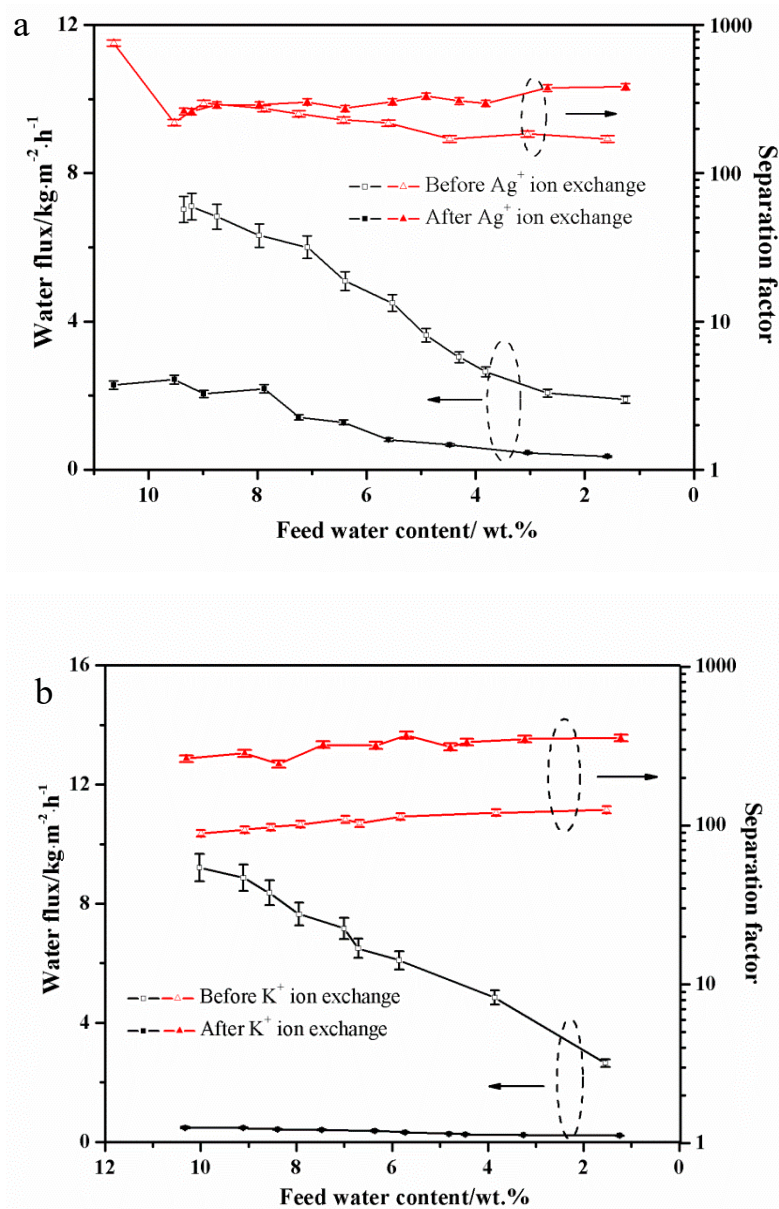
(H<sub>2</sub>, CO<sub>2</sub>, N<sub>2</sub> and CH<sub>4</sub>) were measured by bubble flow meter. As suggested, for the original NaA zeolite membrane, the experimental permeance order followed a Knudsen pattern of H<sub>2</sub> > CH<sub>4</sub> > N<sub>2</sub> > CO<sub>2</sub>. For the smallest gas of H<sub>2</sub>, the permeance reached up to  $7.66 \times 10^{-7} \text{ mol}\cdot\text{m}^{-2}\cdot\text{s}^{-1}\cdot\text{Pa}^{-1}$ , much higher than that for the rest gases of CO<sub>2</sub>, N<sub>2</sub> and CH<sub>4</sub>. For the most strongly adsorbed component of CO<sub>2</sub>, the molecules were anchored in the zeolitic cavities due to dispersive interactions, and the transport was controlled by the molecular movements, thereby leading to a lower CO<sub>2</sub> permeance than that of N<sub>2</sub> and CH<sub>4</sub>, which have higher thermal velocities. After the membrane was treated by AgNO<sub>3</sub> solution, despite the same permeance pattern of gases, all of the permeances were decreased by a factor of 35%. This was because the larger size of Ag<sup>+</sup> (1.26 Å) reduced the accessible pore passage. In comparison, for the membrane that was treated with KCl solution with even larger cation size (K<sup>+</sup> = 1.49 Å), the gas permeance decreased more sharply, and a factor of 90% was found for all of the gases. Since the effect of the hydrophilicity was excluded in gas permeation, the pore narrowing effect was further confirmed. On the other hand, it has been noted that the percentage of permeance drop for gases was more significant than that for the PV dehydration in Table 1. For instance, the drop of permeation flux for the KCl exchanges was only 10% in Table 1, which is far below the value of 90% in gas permeation. Clearly, the smaller decreasing was irrelevant of the variation of the membrane surface hydrophilicities, and it could be mainly attributed to the extra vaporing resistance in the PV operation, where the water molecules escape from the liquid feed to the water vapor phase. Since the permeance difference for PV dehydration is much smaller than that for the gas permeation, so it was reasonable to conclude that the vaporization process of phase change is much more influential than the vapor transport in the zeolite pores. A similar result was also found in the vapor permeation (VP) characterization using different feed mixtures of ethanol/water for Ag<sup>+</sup> and K<sup>+</sup>, where the variation of the permeance and separation factor was provided in Figure 11. As suggested, a greater decreasing percentage of 60% for the permeance was obtained for the vapor mixture with 10 wt % water content, thus confirming that the importance of vaporization resistance in PV dehydration outweighed that of vapor phase transport in the pore channel under current conditions.



**Figure 10.** Gas permeance through (a) the original, (b) the AgNO<sub>3</sub> treated and (c) the KCl solution treated NaA zeolite membrane as a function of the gas kinetic diameter at 25 °C and 2.0 bar.

**Table 5.** The contact angles of the NaA zeolite membrane treated by different cations.

Cation Type	Exchanged NaA Zeolite Membranes	Contact Angle/ $\theta$
Original	NaA zeolite membrane	6.6°
Monovalent cation	Li <sup>+</sup> exchanged NaA zeolite membrane	46.5°
	K <sup>+</sup> exchanged NaA zeolite membrane	43.0°
	Ag <sup>+</sup> exchanged NaA zeolite membrane	99.6°
Divalent cation	Zn <sup>2+</sup> exchanged NaA zeolite membrane	72.6°
	Mg <sup>2+</sup> exchanged NaA zeolite membrane	18.3°
	Ca <sup>2+</sup> exchanged NaA zeolite membrane	46.2°
	Ba <sup>2+</sup> exchanged NaA zeolite membrane	33.5°

**Figure 11.** Vapor permeation (VP) dehydration of different ethanol/water mixtures using salt treated NaA zeolite membrane. (a) AgNO<sub>3</sub> solution and (b) KCl solution, where the vapor pressure was 1.4 bar under a temperature of 100 °C.

#### 4. Conclusions

Different cation-exchanged NaA zeolite membranes were successfully derived on hollow fibers, using monovalent and divalent salts. For the monovalent cations, the membrane showed very stable membrane structure and dehydration performances, except for the very acidic salts of  $\text{NH}_4^+$ , as the dealumination effect occurred in the zeolite frameworks. For the rest monovalent cations of ( $\text{Li}^+$ ,  $\text{K}^+$  and  $\text{Ag}^+$ ), it had been found that the permeation flux variations in dehydration largely related to the cations size. For the smaller sizes, like  $\text{Li}^+$ , a much higher permeation flux was obtained, but the separation factor was completely lost due to the over enlargement of accessible passages that was caused by the replacement of  $\text{Na}^+$  by  $\text{Li}^+$ . For the larger cations, like  $\text{K}^+$  and  $\text{Ag}^+$ , a mild decrement of permeation flux occurred to the treated membrane, but the separation factors became higher for both cations, which was because the accessible passage became narrower. For the divalent cation-treated membrane, the membrane permeance variation was complex, where the permeation flux was generally reduced due to the interplay between the cation size and charges. For larger cation ( $\text{Ba}^{2+}$ ), the PV dehydration performances were slightly reduced for both permeation flux and separation factor, indicating that the membrane intactness was largely maintained and the unbalanced stresses was minimized. For other cations with smaller sizes, both the permeation flux and separation factor were reduced. This was because the number of  $\text{Na}^+$  was unevenly exchanged with  $\text{M}^{2+}$  to balance the charge, so some cation vacancies were left in the treated membrane and thus induced unbalanced stresses in the membrane, thereby damaging the membrane intactness. To further verify the structure variation of the treated membrane by excluding the hydrophilicity factor occurring in the liquid separation, gas permeation using  $\text{H}_2$ ,  $\text{CO}_2$ ,  $\text{N}_2$  and  $\text{CH}_4$  was conducted for the treated NaA zeolite membrane by  $\text{Ag}^+$  and  $\text{K}^+$ , and all of the permeance of gases was found to be decreased, which was consistent with the result that was obtained in the PV dehydration. Thus, the narrowing of the accessible pore channel due to the larger cation replacement in the membrane was firmly validated. However, it has been found that the decrement percentage (90% for  $\text{K}^+$ ) in the gas permeation was far above that for the PV dehydration (10% for  $\text{K}^+$ ), and this could be explained by the higher importance of vaporization resistance of water molecules from liquid to vapor phases, which outweighs the vapor transport resistance in the pore channels in the membrane.

**Author Contributions:** X. Gao and B. Gao conceived and designed the experiments; B. Gao and R. Shi and X. Wang performed the experiments; B. Gao and R. Ur Reshman analyzed the data; X. Gao and X. Gu supervised the project and provided research ideas. X. Gao and B. Gao contributed to the drafting of this paper.

**Acknowledgments:** This work is supported by National Natural Science Foundation of China (51502311), and the Doctorial Programs for Innovation and Entrepreneurship of Jiangsu Province.

**Conflicts of Interest:** The authors declare no conflict of interest.

#### References

1. Zeng, L.; Li, Z. A new process for fuel ethanol dehydration based on modeling the phase equilibria of the anhydrous  $\text{MgCl}_2$  + ethanol + water system. *AIChE J.* **2015**, *61*, 664–676. [[CrossRef](#)]
2. Sanchez, O.J.; Cardona, C.A. Trends in biotechnological production of fuel ethanol from different feedstocks. *Bioresour. Technol.* **2008**, *99*, 5270–5295. [[CrossRef](#)] [[PubMed](#)]
3. Rasmussen, M.L.; Koziel, J.A.; Jane, J.; Pometto, A.L., III. Reducing bacterial contamination in fuel ethanol fermentations by ozone treatment of uncooked corn mash. *J. Agric. Food Chem.* **2015**, *63*, 5239–5248. [[CrossRef](#)] [[PubMed](#)]
4. Seo, D.; Takenaka, A.; Fujita, H.; Mochidzuki, K.; Sakoda, A. Practical considerations for a simple ethanol concentration from a fermentation broth via a single adsorptive process using molecular-sieving carbon. *Renew. Energ.* **2018**, *118*, 257–264. [[CrossRef](#)]
5. Zah, J.; Krieg, H.M.; Breytenbach, J.C. Single gas permeation through compositionally different zeolite NaA membranes: Observations on the intercrystalline porosity in an unconventional semicrystalline layer. *J. Membr. Sci.* **2007**, *287*, 300–310. [[CrossRef](#)]

6. Aoki, K.; Kusakabe, K.; Morooka, S. Preparation of oriented A-type zeolite membranes. *AIChE. J.* **2000**, *46*, 221–224. [[CrossRef](#)]
7. Caro, J.; Noack, M. Zeolite membranes-Recent developments and progress. *Microporous Mesoporous Mater.* **2008**, *115*, 215–233. [[CrossRef](#)]
8. Shao, J.; Zhan, Z.; Li, J.; Wang, Z.; Li, K.; Yan, Y. Zeolite NaA membranes supported on alumina hollow fibers: Effect of support resistances on pervaporation performance. *J. Membr. Sci.* **2014**, *451*, 10–17. [[CrossRef](#)]
9. Wenten, I.G.; Dharmawijaya, P.T.; Aryanti, P.T.P.; Mukti, R.R.; Khoiruddin, K. LTA zeolite membranes: Current progress and challenges in pervaporation. *RSC Adv.* **2017**, *7*, 29520–29539. [[CrossRef](#)]
10. Kita, H.; Horii, K.; Ohtoshi, Y.; Tanaka, K.; Okamoto, K.I. Synthesis of a zeolite NaA membrane for pervaporation of water-organic liquid mixtures. *J. Mater. Sci. Lett.* **1995**, *14*, 206–208. [[CrossRef](#)]
11. Shakarova, D.; Ojuva, A.; Bergstrom, L.; Akhtar, F. Methylcellulose-directed synthesis of nanocrystalline zeolite NaA with high CO<sub>2</sub> uptake. *Materials* **2014**, *7*, 5507–5519. [[CrossRef](#)] [[PubMed](#)]
12. Nikolakis, V.; Xomeritakis, G.; Abibi, A.; Dickson, M.; Tsapatsis, M.; Vlachos, D.G. Growth of a faujasite-type zeolite membrane and its application in the separation of saturated/unsaturated hydrocarbon mixtures. *J. Membr. Sci.* **2001**, *184*, 209–219. [[CrossRef](#)]
13. Cui, Y.; Kita, H.; Okamoto, K.I. Zeolite T membrane: Preparation, characterization, pervaporation of water/organic liquid mixtures and acid stability. *J. Membr. Sci.* **2004**, *236*, 17–27. [[CrossRef](#)]
14. Zhou, R.; Li, J.; Zhu, M.; Hu, Z.; Duan, L.; Chen, X. Synthesis and pervaporation performance of mordenite membranes on mullite tubes. *Chin. J. Inorg. Chem.* **2010**, *26*, 469–475.
15. Yang, S.; Arvanitis, A.; Cao, Z.; Sun, X.; Dong, J. Synthesis of silicalite membrane with an aluminum-containing surface for controlled modification of zeolitic pore entries for enhanced gas separation. *Processes* **2018**, *6*, 13. [[CrossRef](#)]
16. Dincer, E.; Culfaz, A.; Kalipcilar, H. Effect of seeding on the properties of MFI type zeolite membranes. *Desalination* **2006**, *200*, 66–67. [[CrossRef](#)]
17. Korelskiy, D.; Ye, P.; Zhou, H.; Mouzon, J.; Hedlund, J. An experimental study of micropore defects in MFI membranes. *Microporous Mesoporous Mater.* **2014**, *197*, 358. [[CrossRef](#)]
18. Liu, Y.; Wang, X.; Zhang, Y.; He, Y.; Gu, X. Scale-up of NaA zeolite membranes on alpha-Al<sub>2</sub>O<sub>3</sub> hollow fibers by a secondary growth method with vacuum seeding. *Chin. J. Chem. Eng.* **2015**, *23*, 1114–1122. [[CrossRef](#)]
19. Guan, G.; Kusakabe, K.; Morooka, S. Gas permeation properties of ion-exchanged LTA-type zeolite membranes. *Sep. Purif. Technol.* **2001**, *36*, 2233–2245. [[CrossRef](#)]
20. Li, Y.; Chen, H.; Liu, J.; Yang, W. Microwave synthesis of LTA zeolite membranes without seeding. *J. Membr. Sci.* **2006**, *277*, 230–239. [[CrossRef](#)]
21. Li, Y.; Zhou, H.; Zhu, G.; Liu, J.; Yang, W. Hydrothermal stability of LTA zeolite membranes in pervaporation. *J. Membr. Sci.* **2007**, *297*, 10–15. [[CrossRef](#)]
22. Hasegawa, Y.; Nagase, T.; Kiyozumi, Y.; Hanaoka, T.; Mizukami, F. Influence of acid on the permeation properties of NaA-type zeolite membranes. *J. Membr. Sci.* **2010**, *349*, 189–194. [[CrossRef](#)]
23. Caro, J.; Albrecht, D.; Noack, M. Why is it so extremely difficult to prepare shape-selective Al-rich zeolite membranes like LTA and FAU for gas separation? *Sep. Purif. Technol.* **2009**, *66*, 143–147. [[CrossRef](#)]
24. Huang, A.; Caro, J. Cationic polymer used to capture zeolite precursor particles for the facile synthesis of oriented zeolite LTA molecular sieve membrane. *Chem. Mater.* **2010**, *22*, 4353–4355. [[CrossRef](#)]
25. Breck, D.W.; Eversole, W.G.; Milton, R.M.; Reed, T.B.; Thomas, T.L. Crystalline zeolites. I. The properties of a new synthetic zeolite, type A. *J. Am. Chem. Soc.* **1956**, *78*, 5963–5972. [[CrossRef](#)]
26. Shirazian, S.; Ashrafizadeh, S.N. LTA and ion-exchanged LTA zeolite membranes for dehydration of natural gas. *J. Ind. Eng. Chem.* **2015**, *22*, 132–137. [[CrossRef](#)]
27. Varela-Gandia, F.J.; Berenguer-Murcia, A.; Lozano-Castello, D.; Cazorla-Amoros, D. Hydrogen purification for PEM fuel cells using membranes prepared by ion-exchange of Na-LTA/carbon membranes. *J. Membr. Sci.* **2010**, *351*, 123–130. [[CrossRef](#)]
28. Wei, X.; Liang, S.; Xu, Y.; Sun, Y.; An, J.; Chao, Z. Methylcellulose-assisted synthesis of a compact and thin NaA zeolite membrane. *RSC Adv.* **2016**, *6*, 71863–71866. [[CrossRef](#)]
29. Xu, K.; Jiang, Z.; Feng, B.; Huang, A. A graphene oxide layer as an acid-resisting barrier deposited on a zeolite LTA membrane for dehydration of acetic acid. *RSC Adv.* **2016**, *6*, 23354–23359. [[CrossRef](#)]
30. Zhang, Y.; Avila, A.M.; Tokay, B.; Funke, H.H.; Falconer, J.L.; Noble, R.D. Blocking defects in SAPO-34 membranes with cyclodextrin. *J. Membr. Sci.* **2010**, *358*, 7–12. [[CrossRef](#)]

31. Yang, J.; Li, H.; Xu, J.; Wang, J.; Meng, X.; Bai, K.; Lu, J.; Zhang, Y.; Yin, D. Influences of inorganic salts on the pervaporation properties of zeolite NaA membranes on macroporous supports. *Microporous Mesoporous Mater.* **2014**, *192*, 60–68. [[CrossRef](#)]
32. Liu, D.; Zhang, Y.; Jiang, J.; Wang, X.; Zhang, C.; Gu, X. High-performance NaA zeolite membranes supported on four-channel ceramic hollow fibers for ethanol dehydration. *RSC Adv.* **2015**, *5*, 95866–95871. [[CrossRef](#)]
33. Nightingaljer, E.R. Phenomenological the ion solvation. Effective radii of hydrated ions. *J. Phys. Chem.* **1959**, *63*, 1381–1387. [[CrossRef](#)]
34. Shannon, R.D. Revised effective ionic radii and systematic studies of interatomic distances in halides and chalcogenides. *Acta Crystallogr. Sect. A* **1976**, *32*, 751–767. [[CrossRef](#)]



© 2018 by the authors. Licensee MDPI, Basel, Switzerland. This article is an open access article distributed under the terms and conditions of the Creative Commons Attribution (CC BY) license (<http://creativecommons.org/licenses/by/4.0/>).